ecx Documentation

Release 0.1.0

M. Skocic

Oct 27, 2023

CONTENTS:

CHAPTER

ONE

GETTING STARTED

Sources: https://github.com/MilanSkocic/ecx

1.1 ecx

ecx is a Fortran library providing formulas for electrochemistry with a C API.

1.1.1 How to install

The library is built with fpm which will build the fortran code into a static library. An Makefile is provided which uses fpm with additional options for:

- copy the library into the python wrapper folder
- install the C headers
- uninstall the librariy and headers

On windows, msys2 needs to be installed.

Build

```
source configuration
make
```

Run tests

```
fpm test
```

Install

```
make install
```

Uninstall

```
make uninstall
```

1.1.2 Dependencies

```
gcc>=10
gfortran>=10
fpm>=0.7
```

1.1.3 License

GNU General Public License v3 (GPLv3)

1.2 pyecx

Python wrapper around the Fortran ecx library.

1.2.1 How to install

```
.. code-block:: bash

    pip install pyecx
```

1.2.2 Dependencies

```

```

1.2.3 License

GNU General Public License v3 (GPLv3)

1.3 Examples

1.3.1 Example in Fortran

```
program example_in_f
    use iso_fortran_env
    use ecx
    implicit none

    real(real64) :: w(3) = [1.0d0, 1.0d0, 100.0d0]
    real(real64) :: r = 100.0d0
    real(real64) :: p(3) = 0.0d0
    character(len=1) :: e
    integer :: errstat
    complex(real64) :: z(3)

    p(1) = r
    e = "R"
    call ecx_eis_z(p, w, z, e, errstat)
```

(continues on next page)

(continued from previous page)

```
    print *, z


end program
```

1.3.2 Example in C

```c
#include <stdio.h>
#include <stdlib.h>
#include "ecx.h"


int main(void){

    int errstat;
    double w = 1.0;
    double r = 100.00;
    ecx_cdouble z = ecx_cbuild(0.0,0.0);

    ecx_eis_capi_z(&r, &w, &z, "R", 1, 1, &errstat);

    printf("%f I%f \n", creal(z), cimag(z));

    return EXIT_SUCCESS;
}
```

1.3.3 Example in Python

```python
import numpy as np
from pyecx import eis
import matplotlib.pyplot as plt

R = 100
C = 1e-6
w = np.logspace(6, -3, 100)

zr = np.asarray(eis.zr(w, R))
zc = np.asarray(eis.zc(w, C))
zrc = zr*zc / (zr+zc)
print("finish")

fig = plt.figure()
ax = fig.add_subplot(111)

ax.set_aspect("equal")
ax.plot(zrc.real, zrc.imag, "g.", label="R/C")

ax.invert_yaxis()

plt.show()
```

CHAPTER

TWO

THEORETICAL BACKGROUND

2.1 Chemistry

2.1.1 The Debye-Huckel (or ion-cloud) theory of ion-ion interaction

Activity coefficients and ion-ion interactions

Evolution of the concept of an acitivty coefficients

The existence of ions in solution, of interactions between these ions, and of a chemical-potential change $\Delta\mu_{i-I}$ arising from ion-ion interactions have all been taken to be self-evident in the treatment hitherto presented here. This, however, is a modern point of view. The thinking about electrolytic solutions actually developped along different path.

Ionic solutions were at first treated in the same way as nonelectrolytic solutions, though the latter do not contain charged species. The starting point was the classical thermodynamic formula for the chemical potential μ_i of a nonelectrolyte solute

$$\mu_i = \mu_i^0 + RT \ln x_i \tag{2.1.1}$$

In this expression, x_i is the concentration of the solute in mole fraction units, and μ_i^0 is its the chemical potential in the standard state, i.e., when x_i a standard or a normalized value of unity

$$\mu_i = \mu_i^0 \text{ when } x_i = 1 \tag{2.1.2}$$

Since the solute particles in a solution of a nonlectrolyte are uncharged, they do not engage in long-range Coulombic interactions. The short-range interaction arising from dipole-dipole or dispersion forces become significant only when the mean distance between the solute particles is small, i.e., when the concentration of the solute is high. Thus, one can to a good approximation say that there are no between solute particles in dilute nonelectrolyte solutions. Hence, if Eq.2.1.1 for the chemical potential of a solute in a nonelectrolyte solution (with noninteracting particles) is used fot the chemical potential of an ionic species i in an electrolytic solution, then it is tantamount to ignoring the long-range Coulombic interactions between ions. In an actual electrolytic solution, however, ion-ion interactions operate whether one ignores them or not. It is obvious therefore that measurements of the chemical potential μ_i of an ionic species or, rather, measurements of any property that depends on the chemical potential would reveal the error in Eq.2.1.1, which is blind to ion-ion interactions. In other words, experiments show that even in dilute solutions,

$$\mu_i - \mu_i^0 \neq RT \ln x_i \tag{2.1.3}$$

In this context, a frankly empirical approach was adopted by earlier workers not yet blessed by Debye and Huckel's light. Solutions that obeyed Eq.2.1.1 were characterized as *ideal* solutions since this equation applies to systems of noninteracting solute particles, i.e, ideal particles. Electrolytic solutions that do not obey the equation were said to be *nonideal*. In order to use an equation of the form of Eq.2.1.1 to treat nonideal electrolytic solutions, an empirical correction factor f_i was introduced by Lewis as a modifier of the concentration term.

$$\mu_i - \mu_i^0 = RT \ln x_i f_i \tag{2.1.4}$$

It was argued that, in nonideal solutions, it was not just the analytical concentration x_i of species *i*, but its effective concentration $x_i f_i$ which determined the chemical-potential change $\mu_i - \mu_i^0$. This effective concentration $x_i f_i$ was also known as the *activity* a_i of the species *i*, i.e.,

$$a_i = x_i f_i \tag{2.1.5}$$

and the correction factor f_i, as the *activity coefficient*. For ideal solutions, the activity coefficient is unity, and the activity a_i becomes identical to the concentration x_i, i.e.,

$$a_i = x_i \text{ when } f_i = 1 \tag{2.1.6}$$

Thus, the chemical-potential change in going from the standard state to the final state can be written as

$$\mu_i - \mu_i^0 = RT \ln x_i + RT \ln f_i \tag{2.1.7}$$

Eq.2.1.7 summarizes the empirical or formal treatment of the behavior of electrolytic solutions. Such a treatment cannot furnish a theoretical expression for the acitivity coefficient f_i. It merely recognizes that expressions such as Eq.2.1.1 must be modified if significant forces exist between solute particules.

The physical significance of activity coefficients

For a hypothetical system of ideal (noninteracting) particles, the chemical potential has been stated to be given by

$$\mu_i(ideal) = \mu_i^0 + RT \ln x_i \tag{2.1.8}$$

For a real system of interacting particles, the chemical potential has been expressed in the form

$$\mu_i(real) = \mu_i^0 + RT \ln x_i + RT \ln f_i \tag{2.1.9}$$

Hence, to analyze the physical significance of the activity coefficient term in Eq.2.1.9 , it is necessary to compare this equation with Eq.2.1.8. It is obvious that when Eq.2.1.8 is substracted from Eq.2.1.9, the difference is the chemical-potential change $\Delta\mu_{i-I}$ arising from the interactions between the solute particles (ions in the case of electrolytic solutions). That is

$$\mu_i(real) - \mu_i(ideal) = \Delta\mu_{i-I} \tag{2.1.10}$$

and therefore,

$$\Delta\mu_{i-I} = RT \ln f_i \tag{2.1.11}$$

Thus, the activity coefficient is a measure of the chemical-potential change arising from ion-ion interactions. There are several well-established methods of experimentally determining activity coefficients, and these methods are treated in adequate details in standard treatises.

Now, according to the Debye-Huckel theory, the chemical-potential change $\Delta\mu_{i-I}$ arising from ion-ion interactions has been shown to be given by

$$\Delta\mu_{i-I} = -\frac{N_A(z_i e_0)^2}{2\epsilon\kappa^{-1}} \tag{2.1.12}$$

Hence, combining Eq.2.1.12 and Eq.2.1.10, the result is

$$RT \ln f_i = -\frac{N_A(z_i e_0)^2}{2\epsilon\kappa^{-1}} \tag{2.1.13}$$

Thus, the Debye-Huckel ionic-cloud model for ion-ion interactions has permitted a theoretical calculation of activity coefficients resulting in Eq.2.1.13.

The activity coefficient in Eq.2.1.11 arises from the formula Eq.2.1.9 for the chemical potential, in which the concentration of the species *i* is expressed in mole fraction units x_i. One can also express the concentration in

moles per liter of solution (molarity) or in moles per kilogram of solvent (molality). Thus, alternative formulas for the chemical potential of a species *i* in an ideal solution read

$$\mu_i = \mu_i^0(c) + RT \ln c_i \tag{2.1.14}$$

and

$$\mu_i = \mu_i^0(m) + RT \ln m_i \tag{2.1.15}$$

where c_i and m_i are the molarity and molality of the species *i*, respectively, $\mu_i^0(c)$ and $\mu_i^0(m)$ are the corresponding standard chemical potentials.

When the concentration of the ionic species in a real solution is expressed as molarity c_i and molality m_i , there are corresponding activity coefficients γ_c and γ_m and corresponding expressions for μ_i

$$\mu_i = \mu_i^0(c) + RT \ln c_i + RT \ln \gamma_c \tag{2.1.16}$$

$$\mu_i = \mu_i^0(m) + RT \ln m_i + RT \ln \gamma_m \tag{2.1.17}$$

The activity coefficient of a single ionic species cannot be measured

2.2 Kinetics

2.2.1 Nernst potential

2.2.2 Buttler-Volmer

2.3 EIS

2.3.1 Introduction

Frequency dispersion measurements (or impedance spectroscopy) have become a common technique for the study of mass and charge transport in electrochemical systems. With the availability of automated high quality frequency response analysis systems immittance (i.e. impedance or admittance) measurements can be obtained in fairly easy way [1].

The advantage of measurements taken in the frequency domain over measurements in the time domain (i.e. pulse or step response measurements) is that the frequency response earl be described analytically, using an equivalent circuit as model. Time domain analysis often requires the approximation of complex functions, e.g. infinite summations of exponential functions. The circuit elements represent the various (macroscopic) processes involved in the transport of charge and mass. The dispersion relations for most equivalent circuit elements are very simple Barsoukov and Macdonald [1], Orazem and Tribollet [2].

If the (complex) immittance diagrams show distinct features, which can easily be related to specific subcircuits of the equivalent circuit model, analysis become quite simple. Often this can be accomplished by graphical means, using a compass and a ruler. However, if the time constants of the respective subcircuits are close together, or if elements with a fractional (e.g. Warburg, or a CPE-type element, a more sophisticated analysis procedure is needed. As the variation of one circuit parameter can influence large parts of the frequency dispersion, all parameters must be adjusted simultaneously in order to obtain the optimum fit to the data [3, 4, 5]

2.3.2 Black Box Approach

- Assume a black box with two terminals.
- One applies a voltage and measures the current response (or visa versa) as show in Fig. 2.3.1
- Signal can be dc or periodic with frequency math:*f*, or angular frequency $\omega = 2\pi f$ as shown in Fig. 2.3.2

with: $0 \leq \omega < \infty$**:**

- Voltage: $V(\omega) = V_0 \cdot e^{j\omega t}$
- Current: $I(\omega) = I_0 \cdot e^{j(\omega t - \phi)}$

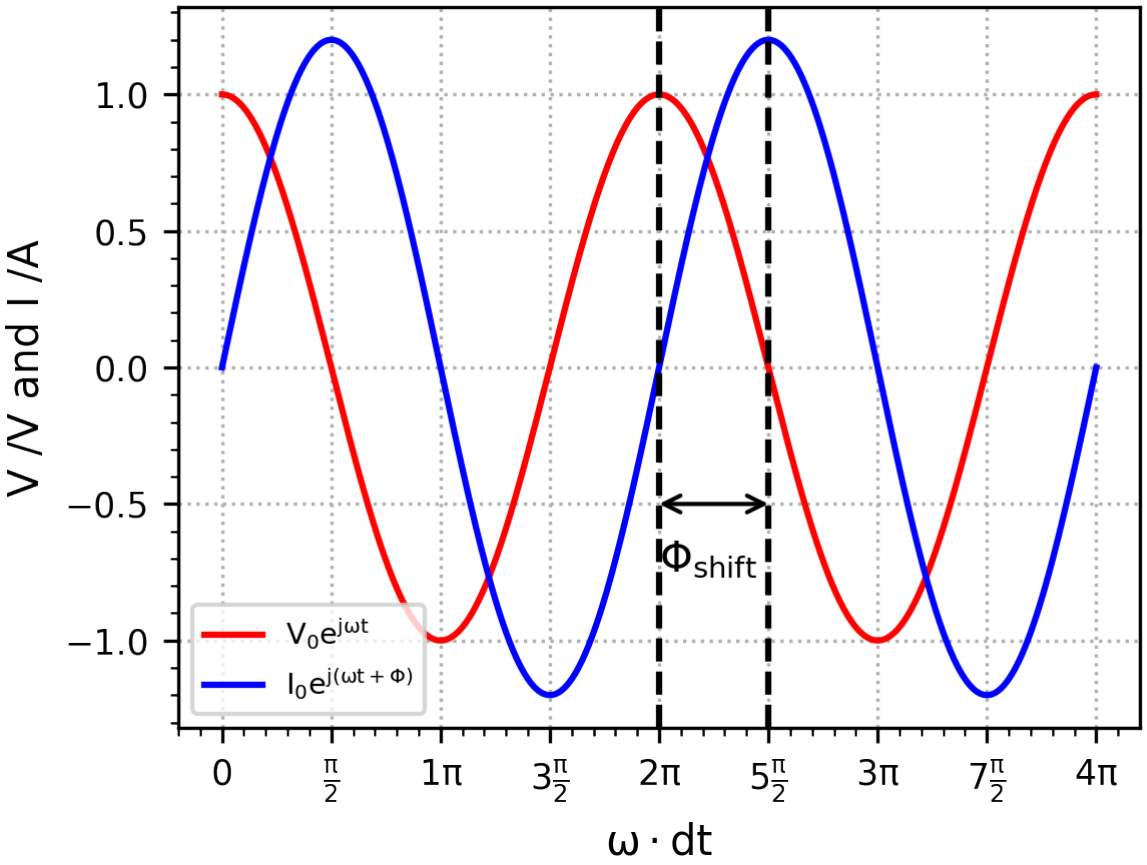

Fig. 2.3.1: EIS AC Waves

2.3.3 What is EIS?

The impedance is determined from the imposed voltage/current and the measured current/voltage through the Ohm's law:

$$Z(\omega) = \frac{V(\omega)}{I(\omega)} = \frac{V_0}{I_0} e^{j\phi} = Z_0 e^{j\phi}$$

Therefore: * Resistive behavior: $ReZ = Z_0 \cdot \cos\phi$ * Capacitive/Inductive behavior $ImZ = Z_0 \cdot \sin\phi$

Sometimes, the complex admittance can also be used which is defined as the inverse of the complex impedance

$$Y(\omega) = \frac{1}{Z(\omega)}$$

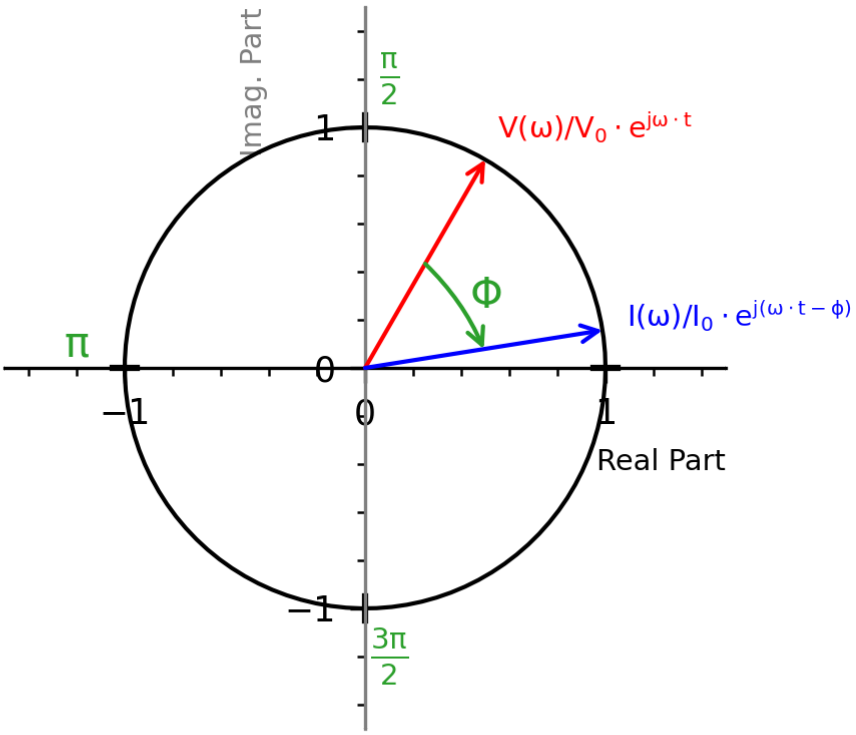

Fig. 2.3.2: Trigonometric Circle

2.3.4 Representation

The impedance $Z(\omega)$ can be represented in two different ways as shown in:

1. **Bode plot**: shows the phase shift and magnitude changes in the applied frequency ranges as shown in Fig. 2.3.4 and Fig. 2.3.5
2. **Nyquist plot**: represents the real and imaginary parts of $Z(\omega)$ using cartesian coordinates as shown in Fig. 2.3.3

The Bode plot has great advantages for observing phase margins in which the system becomes unstable (violent phase or magnitude changes). Therefore, it is useful for the study of sensors, filters, and transistors in electronic devices.

The Nyquist plot provides insight into the possible mechanism or governing phenomena in an equivalent circuit model system. Among these two types of representations, the Nyquist plot is more often used to analyze the characteristics of electrochemical processes.

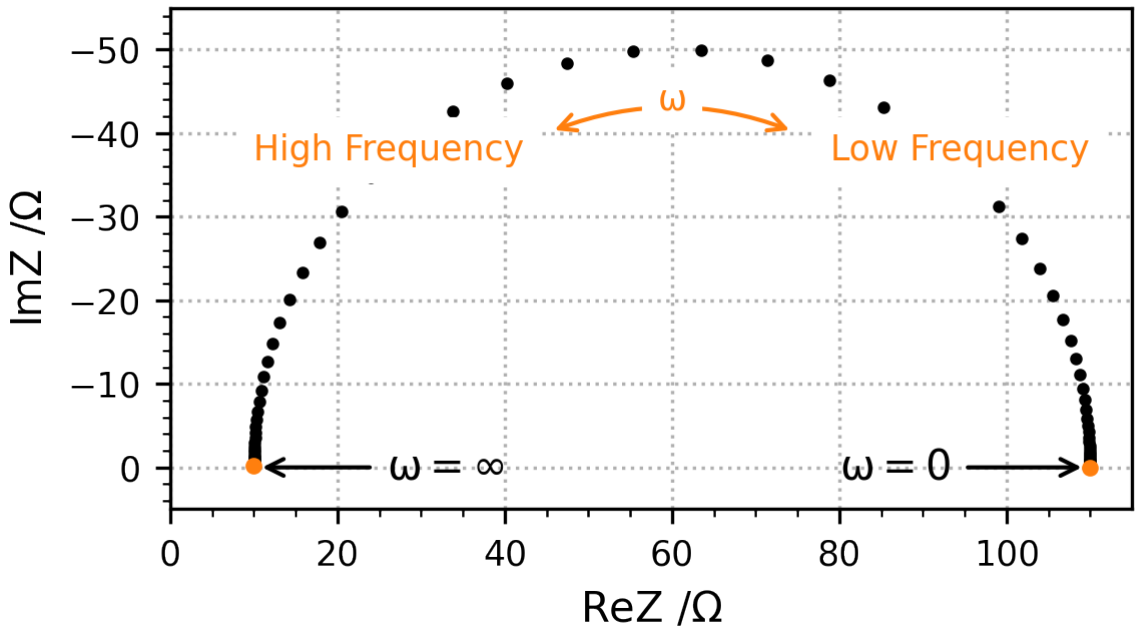

Fig. 2.3.3: Nyquist Representation

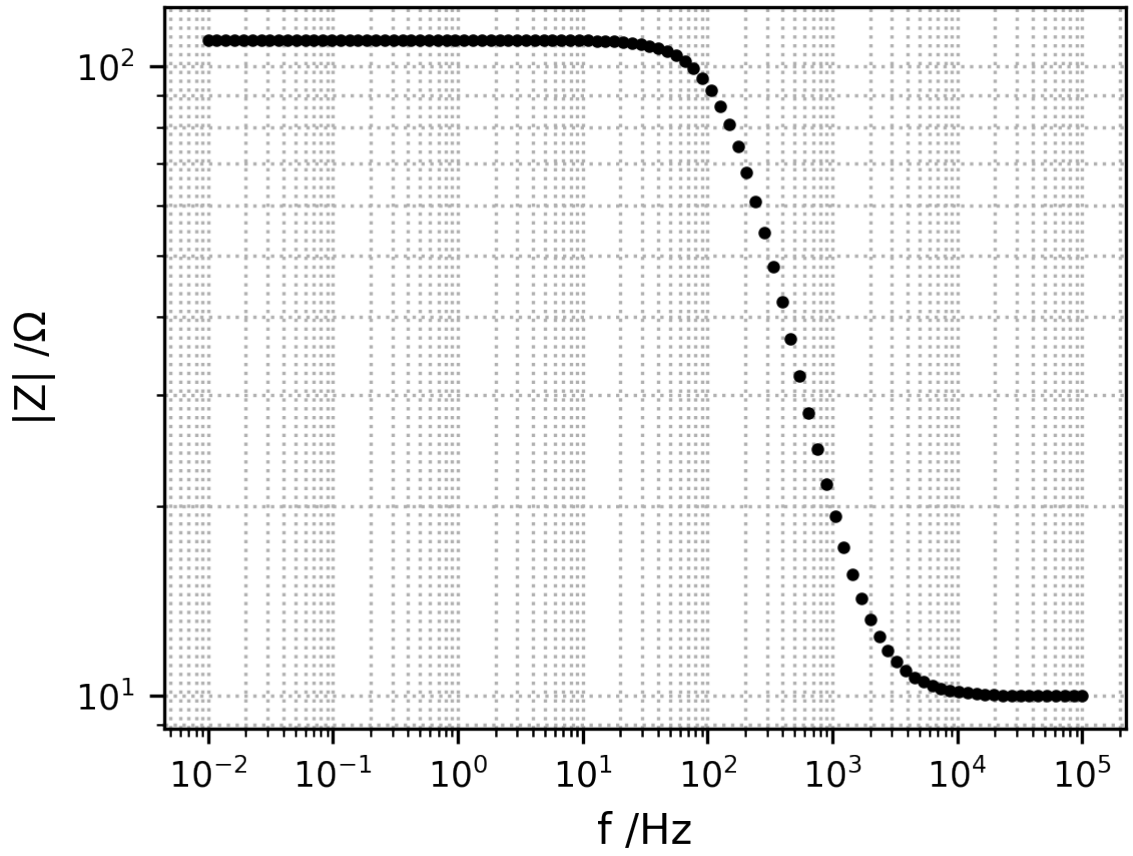

Fig. 2.3.4: Bode Modulus Representation

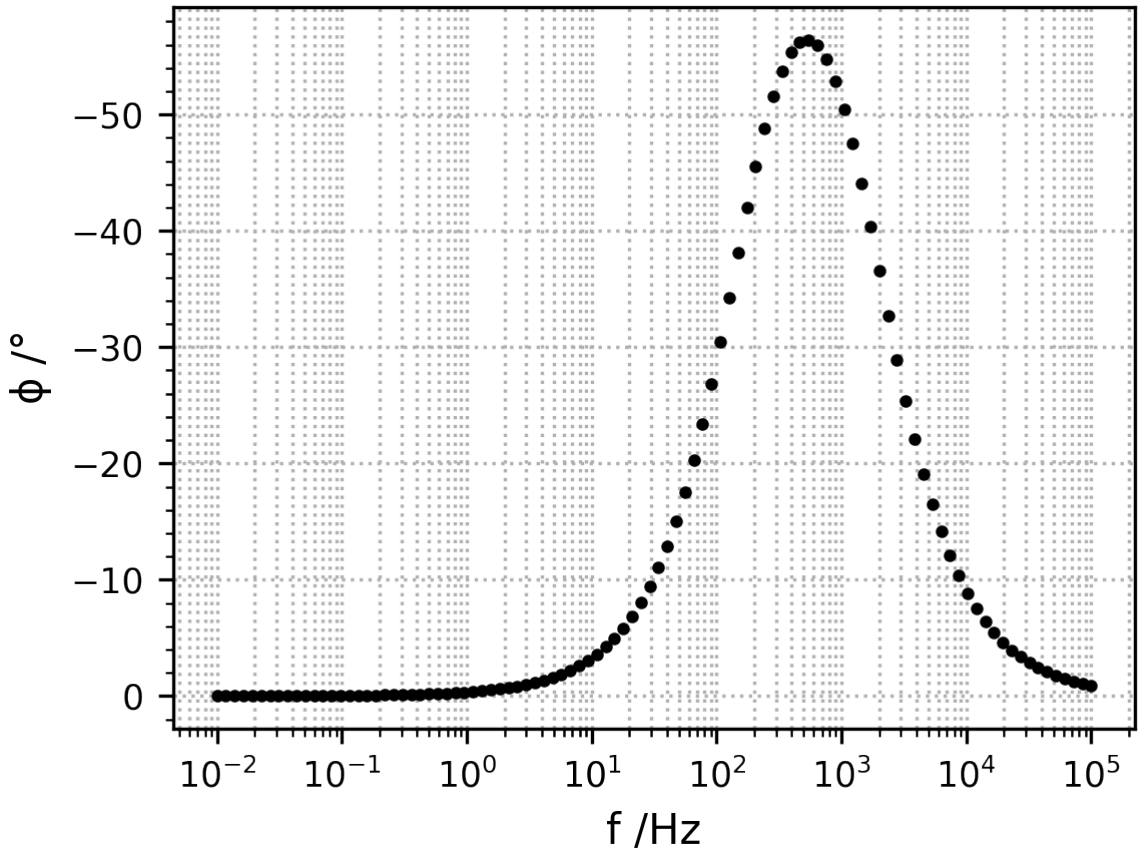

Fig. 2.3.5: Bode Phase Representation

2.3.5 Series and Parallel Connections

- Series connection: $Z_1 - Z_2 - \ldots - Z_n$ = *Z_{eq} = sum Z_i*
- Parallel connection: $Z_1/Z_2/\ldots/Z_n$ = *Z_{eq} = left(sum frac{1}{Z_i} right)^{-1}*

2.3.6 Equivalent Circuit Models

- The circuit model for EIS consists of a combination of electrical circuit elements:
  - ideal elements: resistors (R), capacitors (C) and inductors (L)
  - nonideal capacitor-like element: Constant Phase Element (CPE or Q)
  - diffusion elements: semi-infinite Warburg (W), Finite Length Warburg (W_δ or O) and Finite Space Warburg (W_m or T)
- The circuit model represents the entire system of the electrochemical cell and therefore the aim is to construct an optimal circuit model that is physically meaningful and minimizes the number of variables.

2.3.7 Circuit elements

The differents circuit elements available with their string representation are listed here and their Nyquist representation is shown in Fig. 2.3.6. In order to be recognized by the string parser each element must start the one or two letters defined below and can be followed by a name. The measurement model element needs an additional parameter which the number of Voigt elements defined after an underscore.

- R[name]: $Z(\omega) = R$
- C[name]: $Z(\omega) = \frac{1}{jC\omega}$
- L[name]: $Z(\omega) = jL\omega$
- W[name]: $Z(\omega) = \frac{\sigma}{\sqrt{\omega}} \cdot (1 - j)$
- Wd[name]: $Z(\omega) = \frac{R_\delta \cdot \tanh\left(\sqrt{j\omega\tau}\right)}{\sqrt{j\omega\tau}}$
- Wm[name]: $Z(\omega) = \frac{R_m \cdot \coth\left(\sqrt{j\omega\tau}\right)}{\sqrt{j\omega\tau}}$
- Q[name]: $\frac{1}{Q(jw)^\alpha}$
- M[name]_[n]: $Z(\omega) = R_0 + \sum_{k=0}^{k=n} \frac{R_k}{1+jR_kC_k\omega}$
- G[name]: $Z_G(\omega) = G \cdot (K_g + i\omega)^{-n_g}$

Inductor and Finite Space Warburg are rarely encountered in corrosion studies.

2.3.8 Link between circuit elements and physical parameters

- Resistors can be linked to resistivity or kinetics:
  - $R = \frac{\rho \cdot d}{A}$
  - $R = \frac{RT}{FAj_0(\alpha_a+\alpha_c)} = \frac{RT}{AF^2k^0K_c(\alpha_a+\alpha_c)}$
- Capacitors can be linked to layer thickness
  - $C = \frac{\epsilon\epsilon_0 A}{d}$
- FS/FL Warburg element can be linked to diffusion coefficient and layer thickness:
  - $R = \frac{RT}{AF^2\sqrt{2}} \cdot \frac{d}{D \cdot C^*}$
  - $\tau = \frac{d^2}{D}$

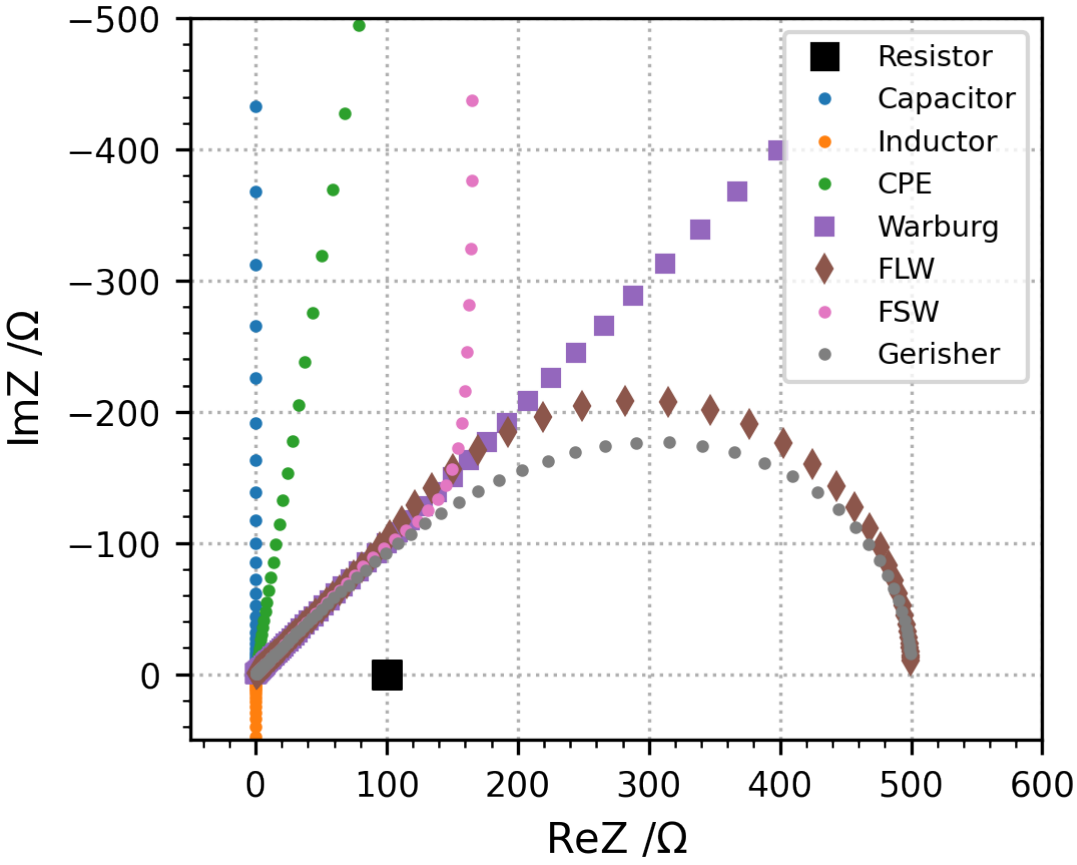

Fig. 2.3.6: Circuit Elements

- $\sigma = \frac{R}{\sqrt{2\tau}}$

where,

- R: resistance [Ω]
- ρ: resistivity [$\Omega \cdot m$]
- d: thickness [m]
- A: Area [m^2]
- j_0: exchange current density [$A \cdot m^{-2}$]
- k^0: kinetics constant [$m \cdot s^{-1}$]
- K_c: concentration factor [$mol \cdot m^{-3}$]
- α_a: anodic transfer coefficient
- α_c: cathodic transfer coefficient
- C^*: bulk concentration of the diffusing species [$mol.m^{-3}$]

2.3.9 Simplified Randles Circuit

Reflects electrochemical reaction controlled only by kinetics as shown in Fig. 2.3.7

- $R_{el} + R_{ct}/C_{dl}$
- R_{el}: electrolyte resistance
- R_{ct}: charge transfer resistance
- C_{dl}: double layer capacitance

2.3.10 Randles Circuit

Reflects electrochemical reaction controlled by kinetics and diffusion as shown in Fig. 2.3.8

- $R_{el} + R_{ct}/C_{dl}$
- R_{el}: electrolyte resistance
- R_{ct}: charge transfer resistance
- C_{dl}: double layer capacitance
- W: semi-infinite diffusion

2.3.11 Differential Impedance analysis

The differential Impedance Analysis (DIA) is based on the use of a Local Operator Model (LOM) which is a equivalent circuit for a simple Faradic reaction but has direct meaning with the experimental spectrum that is being analyzed.

The LOM operator corresponds to the equivalent circuit Rads-(R/C).

The procedure of the structural and parametric identification can be described by the following steps:

- scanning with the LOM throughout the whole frequency range with a scanning window of a single frequency
- parametric identification of the LOM parameters at every working frequency
- Frequency analysis of the LOM parameters' estimates

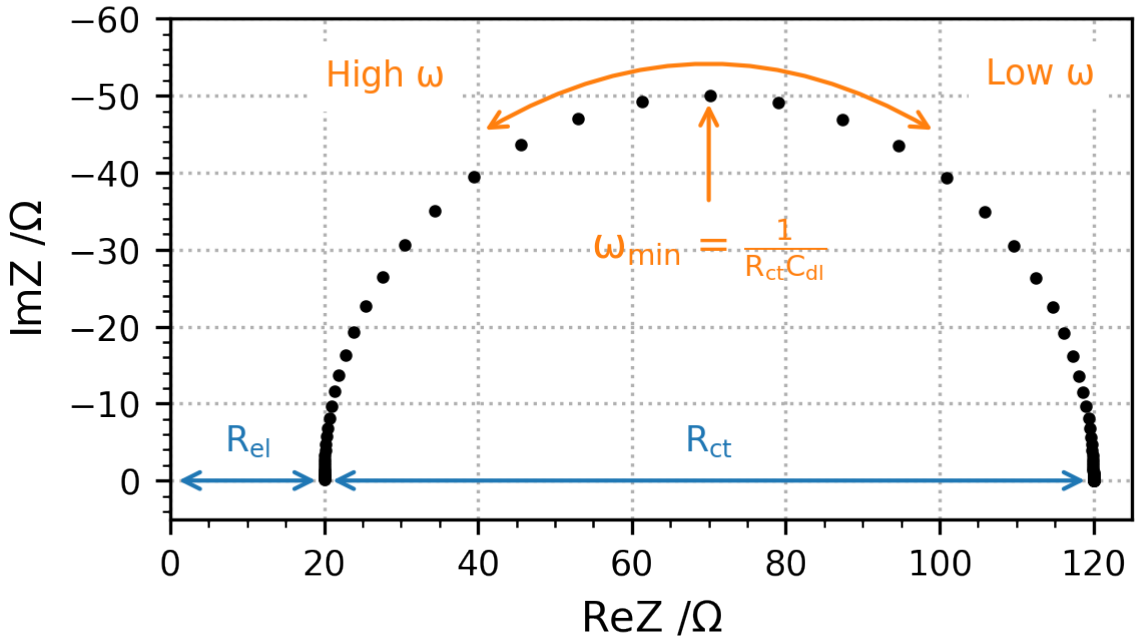

Fig. 2.3.7: Simplified Randles

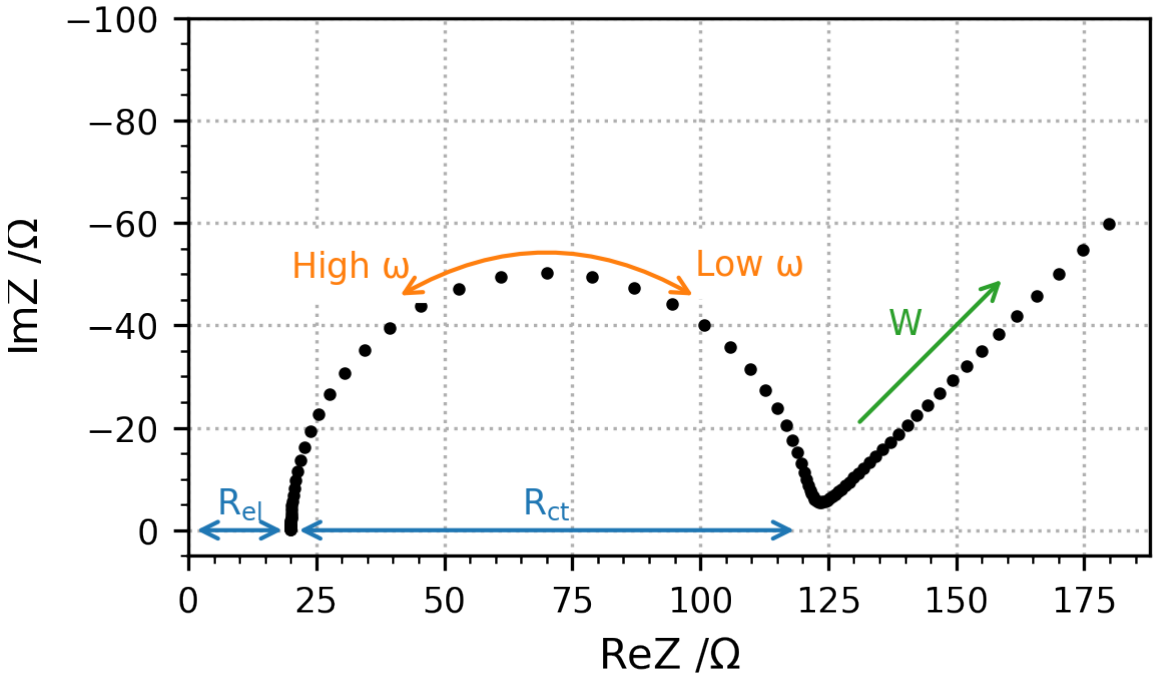

Fig. 2.3.8: Randles

Scanning with the LOM operator

The impedance of the LOM operator is defined as shown in Eq.2.3.1:

$$Z_{LOM} = R_{ads} + \frac{R}{1+T^2\omega^2} - j\frac{\omega RT}{1+T^2\omega^2} \tag{2.3.1}$$

Parametric idenfication of the LOM parameters

The objective is to identify the LOM parameters $P_j = Rads, R, C, T$.

First the effective resistance and the effective inductance are expressed:

$$R_{eff} = ReZ = R_{ads} + \frac{R}{1+T^2\omega^2}$$

$$L_{eff} = -ImZ/\omega = \frac{RT}{1+T^2\omega^2}$$

Derivatives of the effective resistance and inductance are:

$$\frac{dR_{eff}}{d\omega} = -R\frac{2\omega T^2}{(1+T^2\omega^2)^2}$$

$$ImZ = -L_{eff}\cdot\omega$$

$$\frac{dImZ}{d\omega} = -\frac{ImZ}{dL_{eff}}\frac{dL_{eff}}{d\omega} = -\omega\frac{dL_{eff}}{d\omega}$$

$$\frac{dL_{eff}}{d\omega} = -RT\frac{2T^2\omega}{(1+T^2\omega^2)^2} = -\frac{dImZ}{d\omega}\frac{1}{\omega}$$

Expression of the LOM parameters P_i:

$$T(\omega) = \frac{\frac{dL_{eff}}{d\omega}}{\frac{dR_{eff}}{d\omega}} = \frac{dL_{eff}}{dR_{eff}}$$

$$R(\omega) = -\frac{dR_{eff}}{d\omega}\cdot\frac{(1+T^2\omega^2)^2}{2\omega T^2}$$

$$R_{ads}(\omega) = R_{eff}(\omega) - \frac{R}{1+T^2\omega^2}$$

$$C(\omega) = \frac{T}{R}$$

Temporal analysis

The temporal analysis computes the logarithmic values of the LOM parameters $L_j = a, r, c, t$ with respect to ν as defined in Eq.2.3.2:

$$\begin{aligned} L_j = \log_{10} P_j = \log_{10} Rads, \log_{10} R, \log_{10} C, \log_{10} T \\ L_j = a, r, c, t \\ \nu = \log_{10}\frac{1}{\omega} \end{aligned} \tag{2.3.2}$$

Differential temporal analysis

The differential temporal analysis computes the derivatives d_j of L_j with respect to ν as defined in Eq.2.3.3

$$d_j = \frac{dL_j}{d\nu} = da, dr, dc, dt \tag{2.3.3}$$

Spectral analysis

The spectral analysis is obtained by accumulating frequency bands with approximatively equal values of the parameters L_j. The amplitude of the individual spectral line $S_{j,l}$ can be expressed as shown in Eq.2.3.4.

$$\begin{aligned} S_{j,l} &= \sum_{1}^{N} B(L_{j,i}) \\ B(L_{j,i}) &= w_0 \text{ if } l < L_{j,l} < l + s \\ B(L_{j,i}) &= 0 \text{ otherwise} \\ w_0 &= N_{frequencies}/N_{decades} \end{aligned} \tag{2.3.4}$$

The spectral line is expressed in dB.

Differential spectral analysis

The differential spectral analysis is obtained by accumulating frequency bands with approximatively equal values of the parameters d_j. The amplitude of the individual spectral line $S_{j,l}$ can be expressed as shown in Eq.2.3.5.

$$\begin{aligned} S_{j,l} &= \sum_{1}^{N} B(d_{j,i}) \\ B(d_{j,i}) &= w_0 \text{ if } l < d_{j,l} < l + s \\ B(d_{j,i}) &= 0 \text{ otherwise} \\ w_0 &= N_{frequencies}/N_{decades} \end{aligned} \tag{2.3.5}$$

The spectral line is expressed in dB.

An example with a simple RC circuit:

2.4 PEC

2.4.1 Introduction

PEC takes advantage of the photovoltaic effect, discovered by Becquerel [6] in 1839, that occurs at the interface of a semiconductor and an electrolyte. In fact, the first experience showed the occurence of a photopotential and a photocurrent under illumination when a silver electrode, covered with an oxide layer, was immersed in an acidic medium and connected to a platinum electrode. Nonetheless, the first studies focused on the understanding of the interfacial processes were performed much later [7, 8, 9].

The basics of photoelectrochemistry and application examples are presented here and they are largely described in the literature [10, 11, 12, 13, 14, 15]. Several hypotheses are needed in order to apply the theoretical concepts:

- semiconductors are considered to be ideal i.e. crystalized and homogeneous
- the dielectric constant of the semiconductor is independent of the light wavelength
- the capacity of the Helmholtz layer is greater than the capacity of the space charge capacitance
- the potential drop in the Helmholtz layer is independent of the applied potential and is negligible

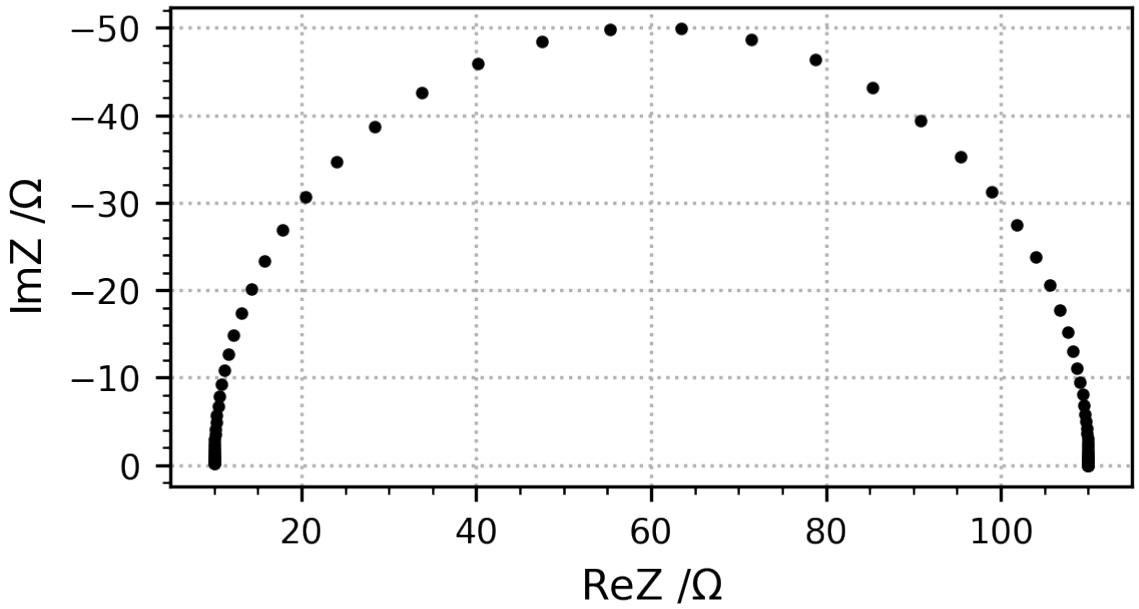

Fig. 2.3.9: Simple RC

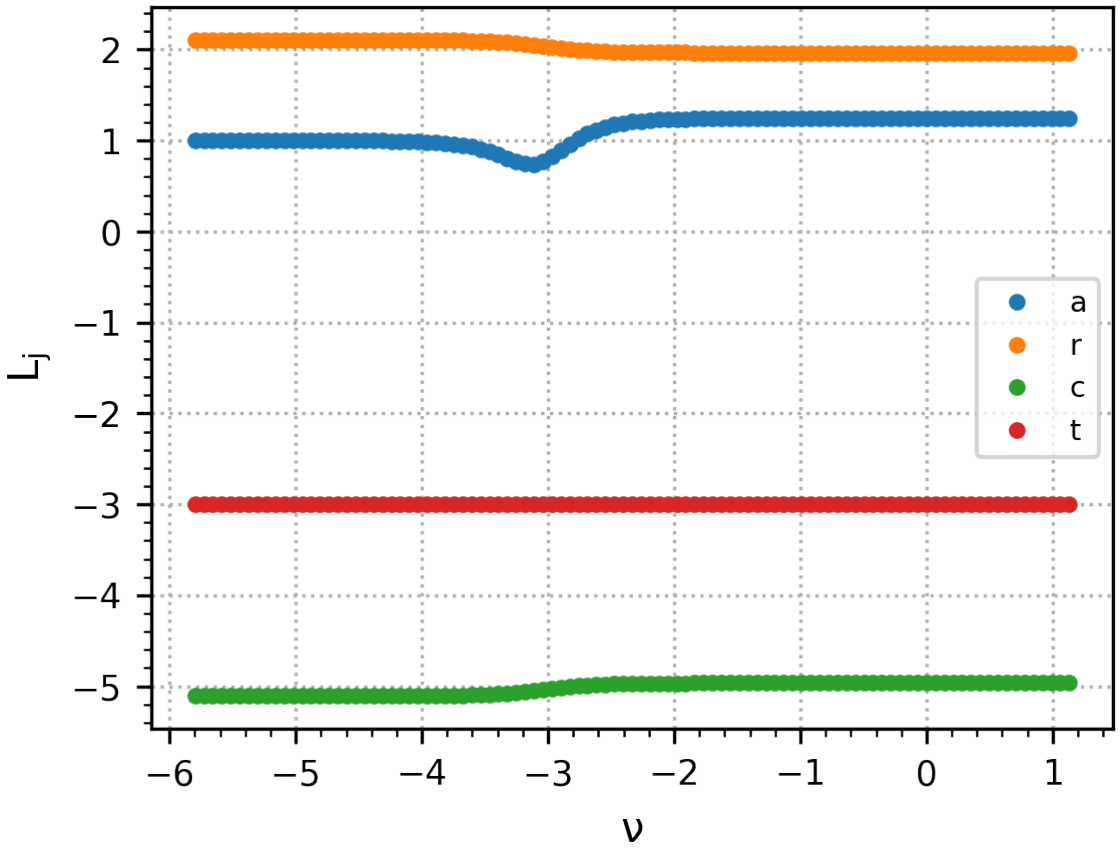

Fig. 2.3.10: Temporal Analysis

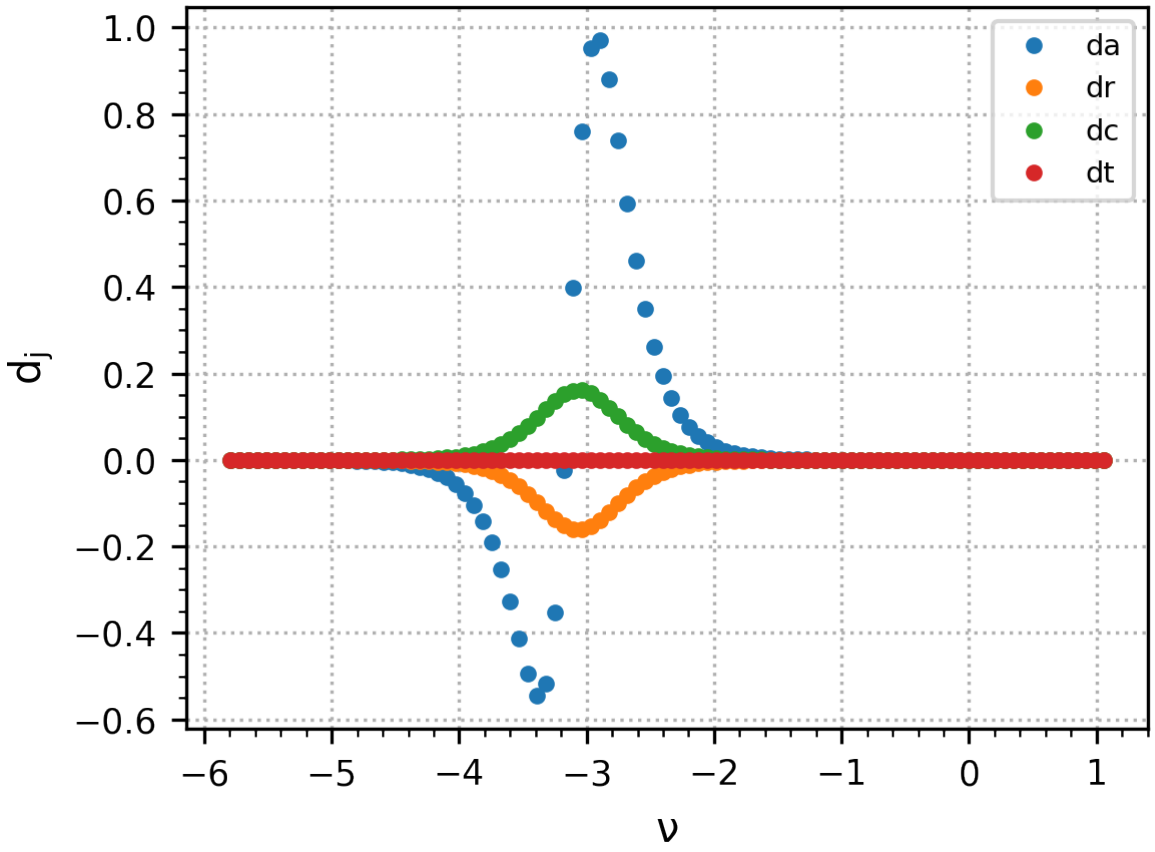

Fig. 2.3.11: Differential Temporal Analysis

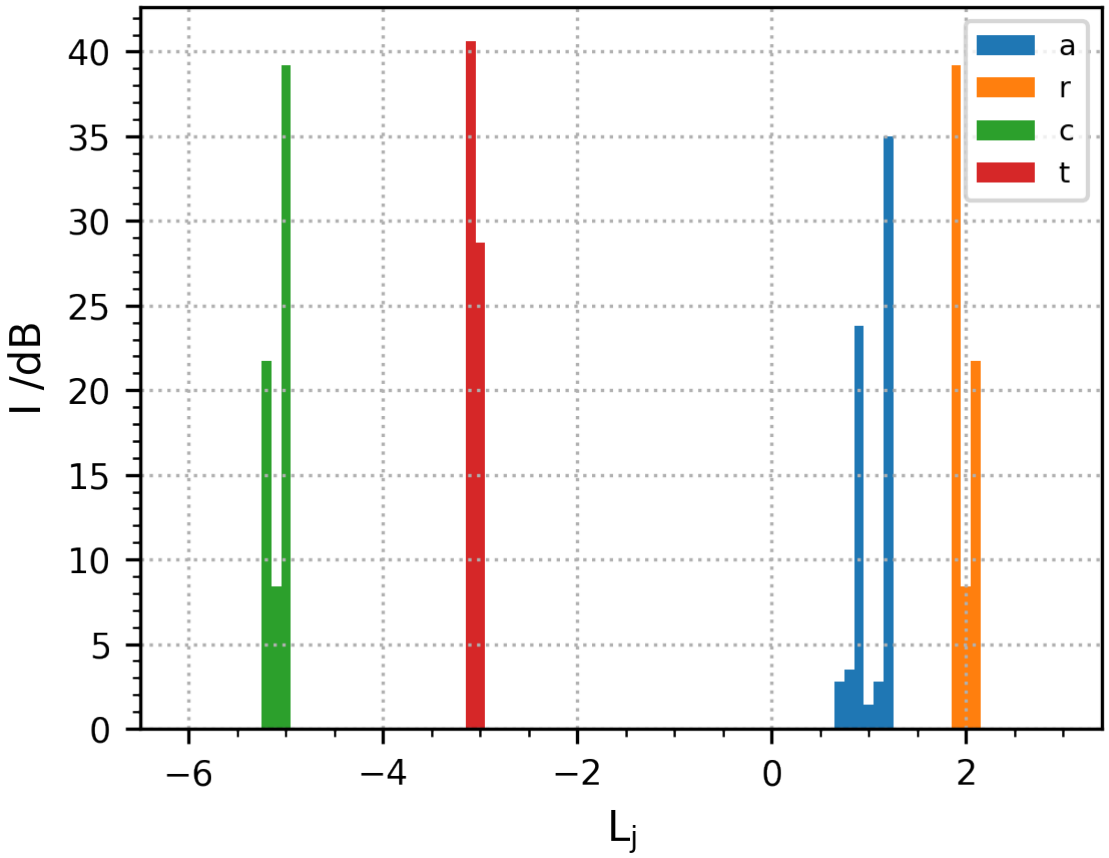

Fig. 2.3.12: Spectral Analysis

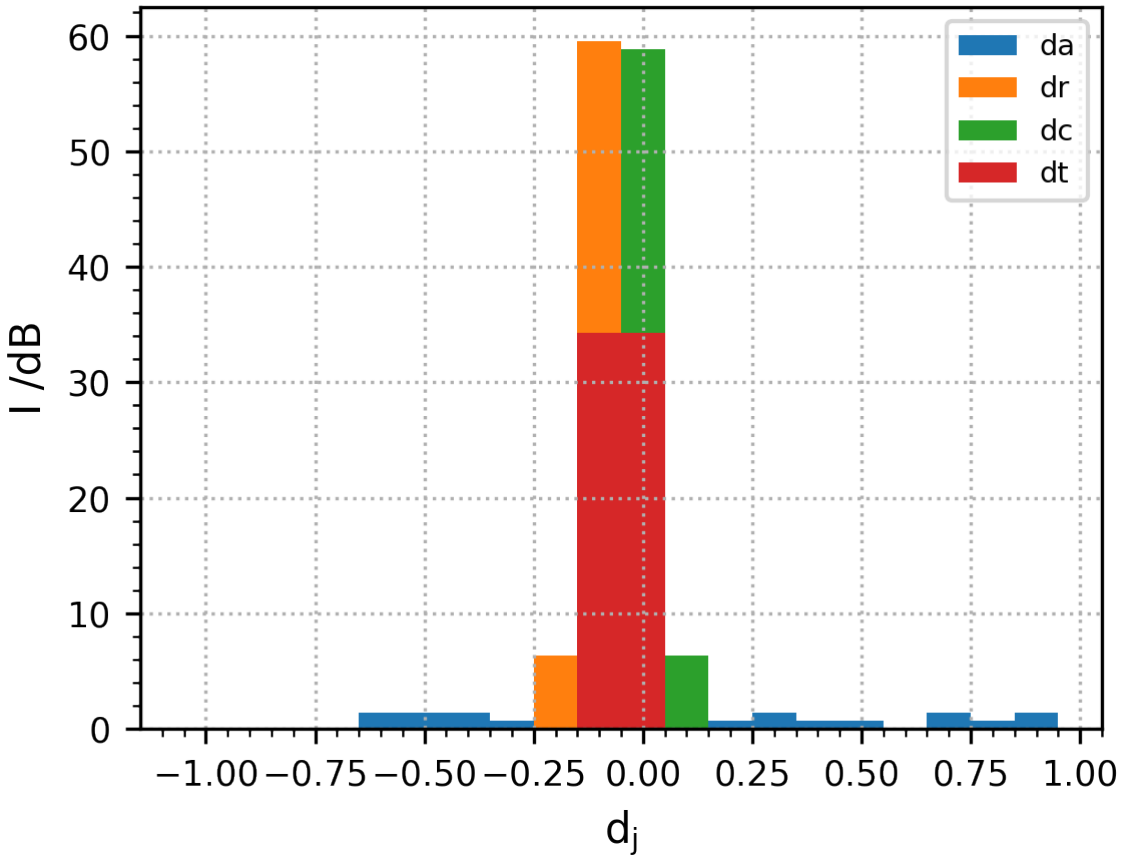

Fig. 2.3.13: Differential Spectral Analysis

The hypotheses are rarely fully respected in the case of oxides or passive films formed on common alloys. Nonetheless, the literature shows that the developed models can be applied to non-ideal systems such as oxides or passive layers.

Solids are generally classified into three groups: *condcutors*, *semiconductors* and *insulators*. Each category can be illustrated with a specific band structure as shown in figure Fig. 2.4.1 [16]. Valence and conduction bands correspond to the allowed energy states for the electrons. The lowest energy level of the conduction band is labeled E_c and the highest energy level of the valence is labeled E_v. They are separated by a band gap, E_g, with no allowed energy states. The repartition of the electrons among both bands are described by the position of the Fermi level, E_F, which represents the highest energy state that can be occupied at 0K.

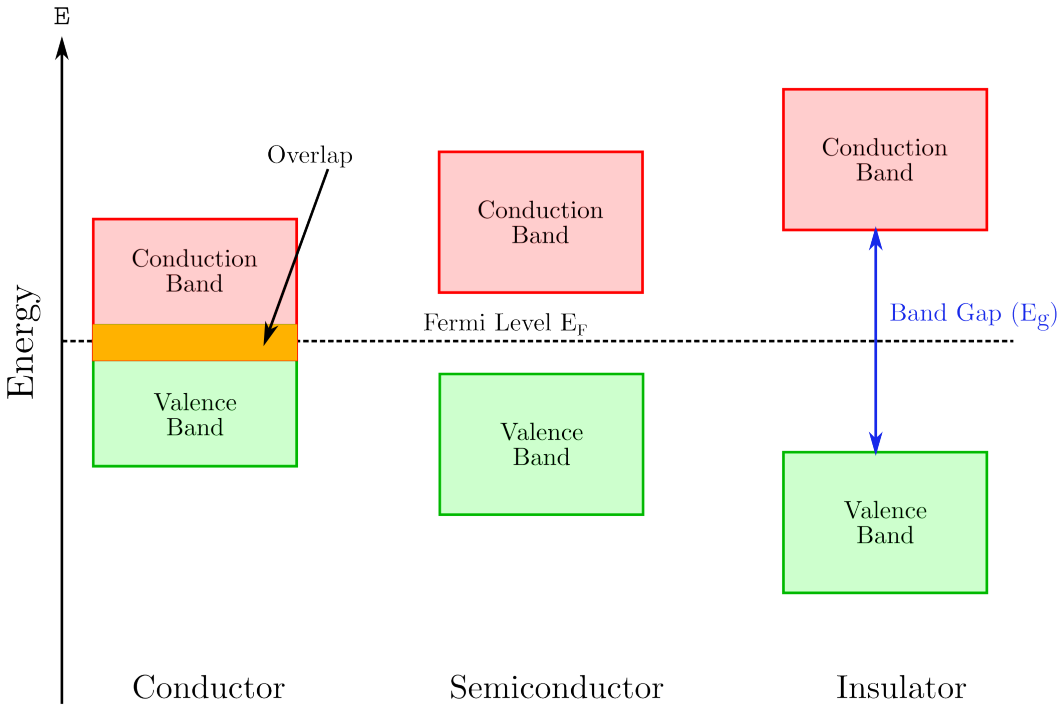

Fig. 2.4.1: Band Structure

The electronic conduction is due to the movement either of the negatively charge electrons in the conduction band or the positively charged holes in the valence band or both simultaneously. Consequently, the conduction depends on the number of available charge carriers in the conduction and valence bands. In conductors, an overlap of the conduction and the valence bands occurs which means that the highest allowed energy band is partilly filled. The distinction between a semiconductor and an isolator is less obvious because the conduction depends on the band gap and the energy provided by the environment to the electron from the valence band in order to jump into the conduction band.

In semiconductors, charge carriers can be generated by three mechanisms: *thermal*, *excitation*, *photoexcitation*, *doping*, as shown in figure Fig. 2.4.2.

In the case of very low band gaps, thermal excitation can be enough to eject an electron from the valence band into the conduction band. Photoexcitation ejects electrons from the valence band into the conduction band when an incident photon, with an energy greater than the band gap, is absorbed. Doping introduces additional energy levels located in between the conduction and valence bands.

Doping occurs when the stoichiometry is altered or when impurities are introduced in the crystallographic lattice of the semiconductor. In the case of n-type semiconductors, the donor energy levels E_d lie just under the conduction

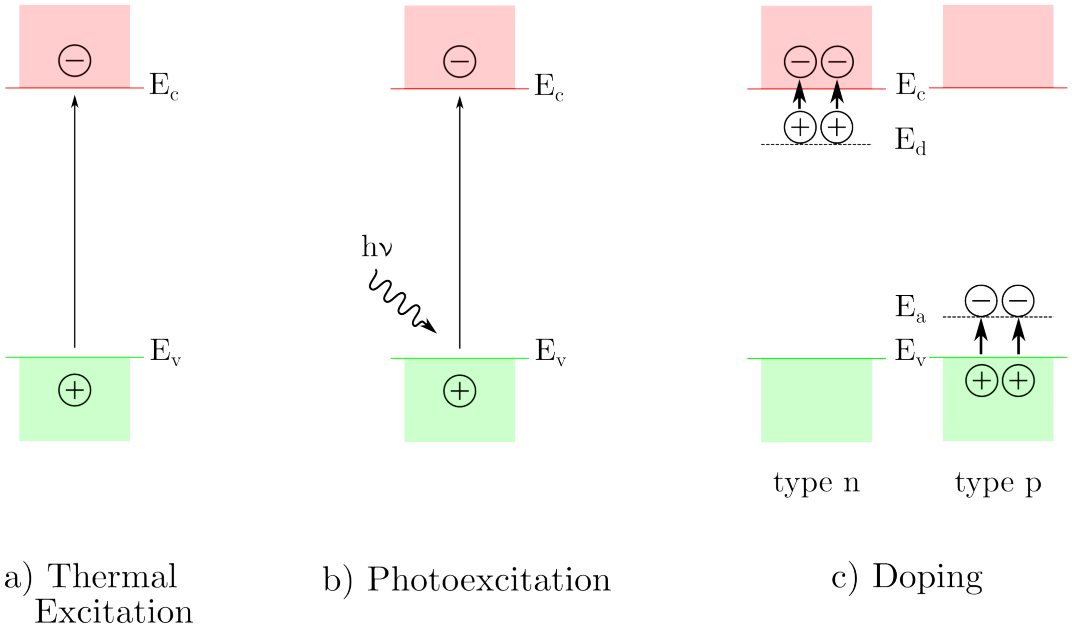

Fig. 2.4.2: Schematic representation of the mechanisms generating charge carriers in semiconductors

band. The electrons from the donor levels are ejected by thermal excitation. Consequently, the majority charge carriers are negatively charged electrons in the conduction band. Similarly, the acceptor energy levels E_a, of p-type semiconductors, lie just above the valence band. The latter trap electrons from the valence band and therefore create holes. Consequently, the majority charge carriers are positively charged holes.

The Fermi level E_F in intrinsic semiconductors is located at the mid-gap. The n-type and p-type doping shift the Fermi level towards band edges E_c and E_v, respectively. The figure Fig. 2.4.3 shows the position of the Fermi level with respect to the semiconductor types.

2.4.2 Semiconductor/electroyte interface in dark

A potential gradient occurs when a semiconductor comes into contact with an electrolyte as shown in figure Fig. 2.4.4.

The position of the Fermi level in the electrolyte with respect to the conduction and valence band edges leads to three different situations after a transient charge transfer. The flat band occurs when the Fermi level in the electrolyte matches the Fermi level in the semiconductor. Consequently, there is no potential gradient in the semiconductor. In a case of Fermi level mismatch, a band bending occurs in the semiconductor near the semiconductor/electrolyte interface. The band bending leads to either depletion or accumulation of majority charge carriers near the semiconductor/electrolyte interface. The spatial extension of the depletion/accumulation zone is called space charge as shown in figure Fig. 2.4.5.

Depletion and accumulation as well as band bending can be obtained by polarizing the semiconductor. As long as the hypothesis described in the introduction paragraph stand, the polarization does not modify the surface band edges E_{cs} and E_{vs}. Consequently, the polarization will only alter the band bending in the space charge. Depending on the applied potential, U, with respect to the flat band, U_{fb}, three different situations will occur:

- $U = U_{fb}$: flat band situation no matter the semiconductor type
- $U > U_{fb}$: depletion (accumulation) in a case of n-type (p-type) semiconductor
- $U < U_{fb}$: accumulation (depletion) in a case of p-type (n-type) semiconductor

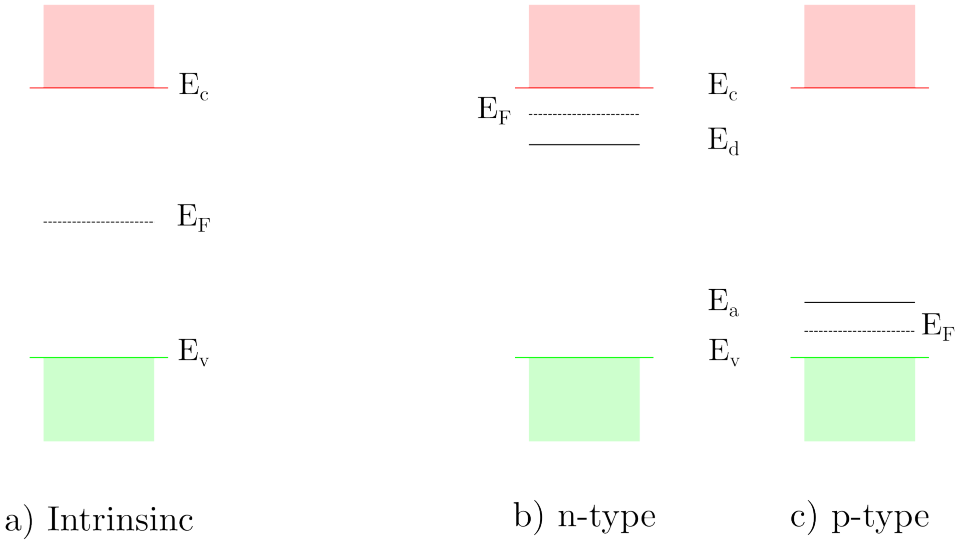

Fig. 2.4.3: Schematic representation of the Fermi level position

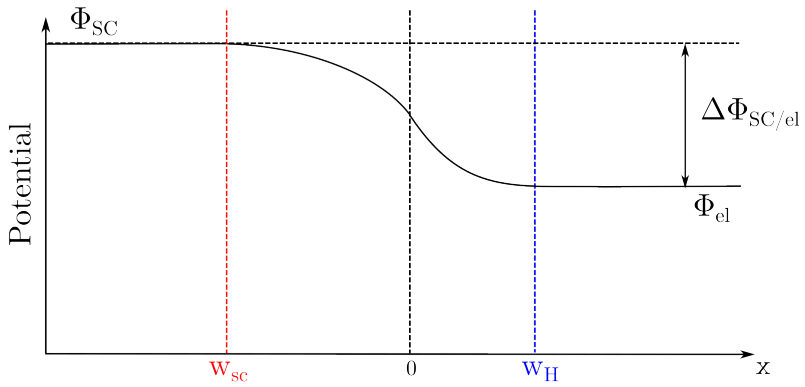

Fig. 2.4.4: Schematic representation of the interfacial gradient potential

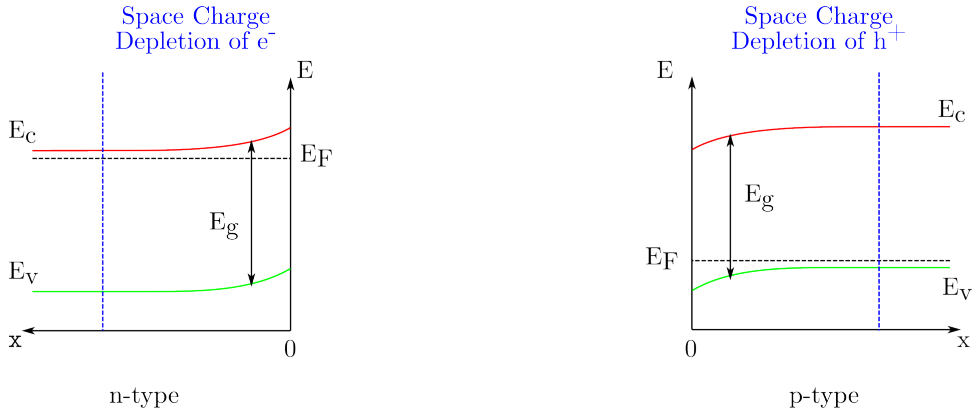

Fig. 2.4.5: Schematic representation ofthe space charge

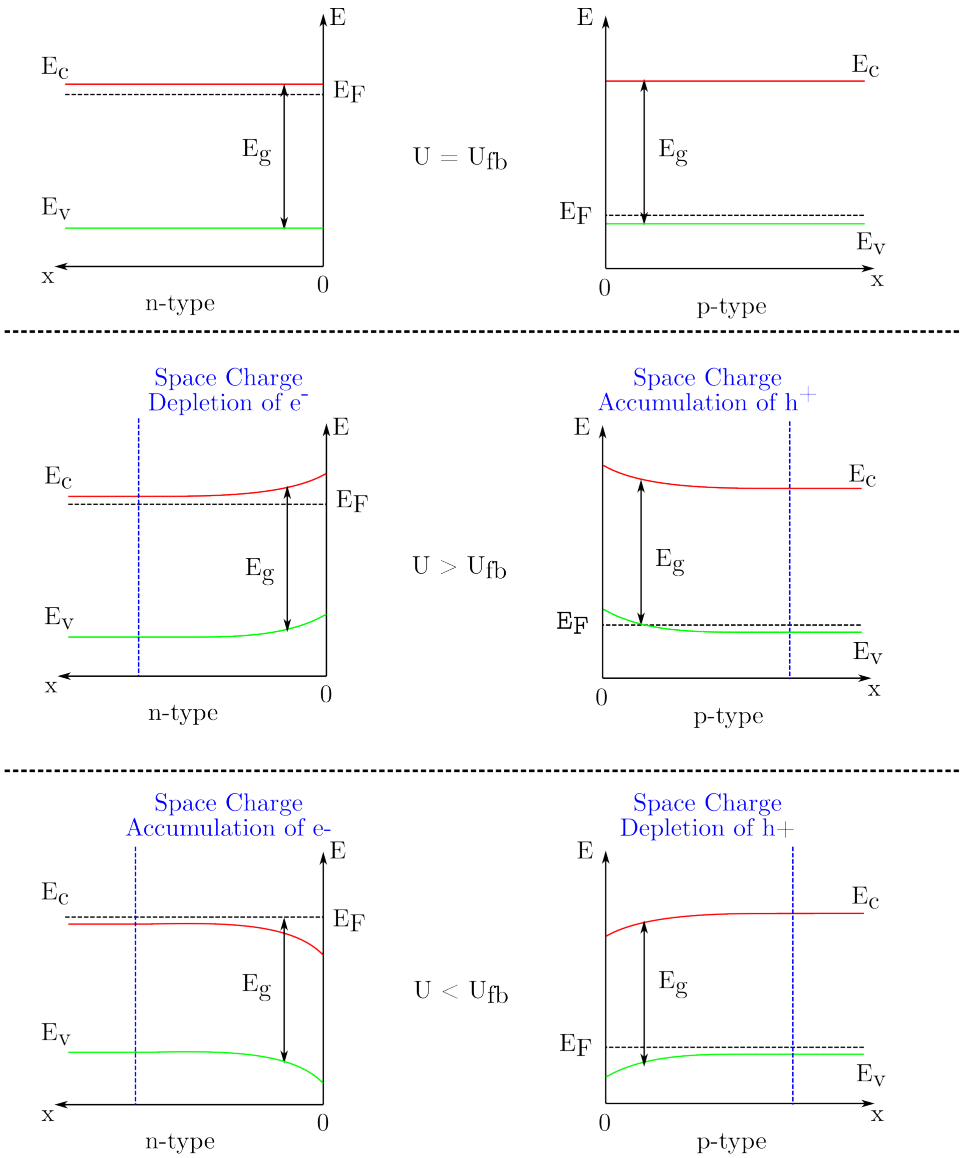

Fig. 2.4.6: Schematic representation of the band bending in p-type and n-type semiconductors.

Without illumination, cathodic (anodic) currents are favored in a case of accumulation of electrons (holes) for an n-type (p-type) semiconductor. In fact, the majority charge carriers of n-type (p-type) semiconductors are electrons (holes). Reciprocally, anodic (cathodic) currents are not favored in a case of depends of electrons (holes) for an n-type (p-type) semiconductor. The junction between a semiconductor and an electrolyte acts like a Schottky diode.

2.4.3 Semiconductor/electroyte interface under illumination

The illumination of the semiconductor/electrolyte interface, with photons having an energy greater than the band gap, E_g, creates electron/hole pairs in the semiconductor. By applying the adequate potential the pairs can be separated. As a consequence, the majority charge carriers are attracted to the semiconductor bulk whereas the minority charge carriers are drawn to the semiconductor/electrolyte interface where they can be transferred to a RedOx species creating an additional current called photocurrent.

Figure Fig. 2.4.7 illustrates schematically the mechanism leading to the creation of a photocurrent. n-type (p-type) semiconductors generate anodic (cathodic) photocurrents where the electrons (holes) move towards the external circuit whereas the holes (electrons) move towards the interface. The photocurrent is significant when the semiconductor/electrolyte junction is in depletion. Therefore, the applied potential on n-type (p-type) semiconductors is greater (lower) than the flat band potential.

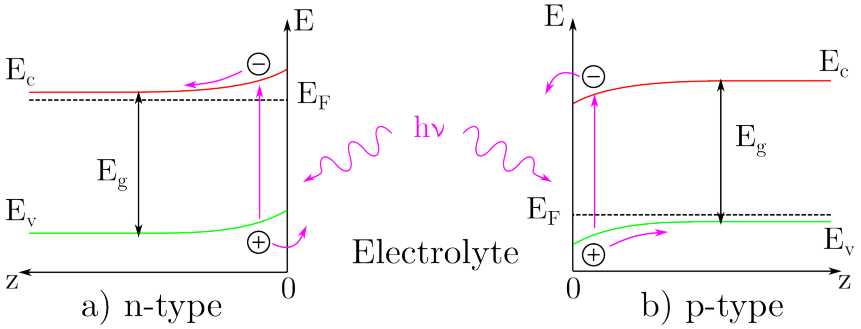

Fig. 2.4.7: Schematic representation of the mechanism generating a photocurrent.

Figure Fig. 2.4.8 and Fig. 2.4.9 show the anodic (cathodic) photocurrent for a GaAs n-type (p-type) semiconductor.

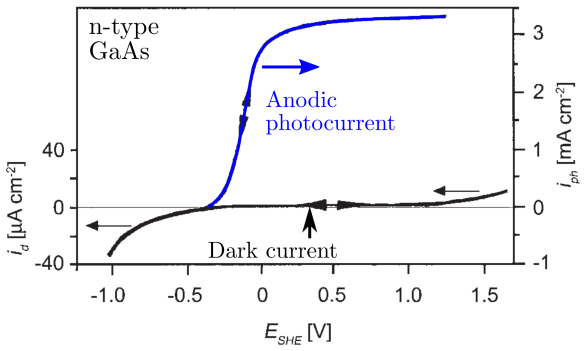

Fig. 2.4.8: Anodic photocurrent for n-type GaAs.

Gärtner [17] and Butler [18] proposed a simple and robust model for describing the photocurrent considering that the recombination of the photogenerated electron/hole pairs does not occur in the space charge. Therefore, the photocurrent is proportional to the photon flux Φ_0. Moreover, the photocurrent depends on the relative ratio between the space charge width, w_{sc}, the depth of penetration given by the inverse of the absorption coefficient, α and the average diffusion length, L_{sc}, of the minority charge carriers. In other words, all absorbed photons generate

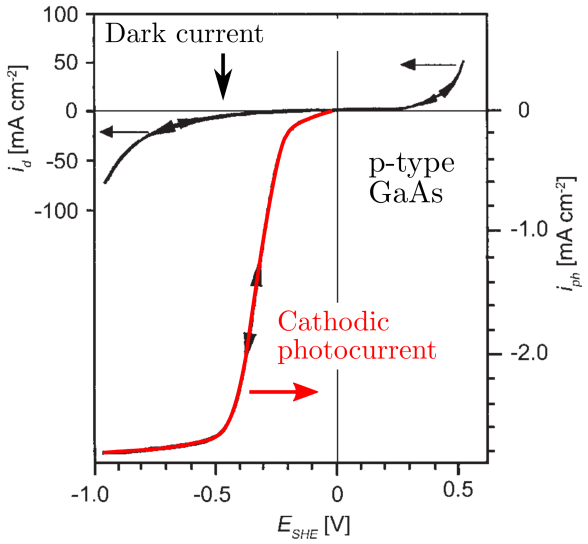

Fig. 2.4.9: Cathodic photocurrent for p-type GaAs.

electron/hole pairs and the minority charge carriers are transferred to the electrolyte and therefore contribute to the photocurrent whose expression is given by the equation Eq.2.4.1.

$$I_{ph} = \Phi_0 \left[1 - \frac{\exp(-\alpha_{sc} \cdot w_{sc})}{1 + \alpha_{sc} \cdot L_{sc}}\right] \tag{2.4.1}$$

When $\alpha_{sc} \cdot w_{sc} << 1$ and $\alpha_{sc} \cdot L_{sc} << 1$, the photocurrent is approximated by the equation Eq.2.4.2.

$$I_{ph} = \Phi_0 \cdot \alpha_{sc} \cdot w_{sc} \tag{2.4.2}$$

The expression of the space charge width, w_{sc}, in depletion is given by the equation Eq.2.4.3 according to the Mott-Schottky theory. N_{cc} represents the number of majority carriers, supposed to be equal to the doping, e corresponds to the elementary charge of an electron, U represents the applied potential, U_{fb} represents the flat band potential, ϵ and ϵ_0 represent the relative and the vacuum permittivity, respectively.

$$w_{sc} = \sqrt{\frac{2\epsilon\epsilon_0}{eN_{cc}} \cdot \left(U - U_{fb} - \frac{kT}{e}\right)} \tag{2.4.3}$$

The expression of the absorption coefficient α_{sc} with respect to the light energy $h\nu$ is shown in equation Eq.2.4.4. The value of n depends on the band-band transition type. n takes discreet values 0.5 or 2 when direct or indirect transitions are allowed, respectively.

$$\alpha_{sc} = C \cdot \frac{(h\nu - E_g)^n}{h\nu} \text{ with } C = \text{constant} \tag{2.4.4}$$

The complete expression of the photocurrent is therefore given by the equation Eq.2.4.5. The latter is obtained by substituting the absorption coefficient α_{sc} and the space charge width w_{sc} from the equation Eq.2.4.2 by the equations Eq.2.4.3 and Eq.2.4.4.

$$I_{ph} = \Phi_0 \cdot C \cdot \frac{(h\nu - E_g)^n}{h\nu} \text{ with } \cdot \sqrt{\frac{2\epsilon\epsilon_0}{eN_{cc}} \cdot \left(U - U_{fb} - \frac{kT}{e}\right)} \tag{2.4.5}$$

The linear transform with respect to the energy of the equation Eq.2.4.5 is shown in equation Eq.2.4.6 and it is used for determining the band gaps. The linear transform with respect to the potential is shown in equation Eq.2.4.7 and it is used for determining the semiconduction type, the flat band potential and the number of majority charge carriers.

$$\left[\frac{I_{ph} \cdot h\nu}{\Phi_0}\right]^{1/n} = C \cdot (h\nu - E_g) \tag{2.4.6}$$

$$I_{ph}^2 = C \cdot \left(U - U_{fb} - \frac{kT}{e}\right) \tag{2.4.7}$$

CHAPTER

THREE

RELEASE NOTES

3.1 ecx 0.1.0 Release Note

3.1.1 Changes

- Implementation of eis + C API
- Python wrappers for eis.
- Documentation with sphinx.

3.1.2 Download

ecx

pyecx

3.1.3 Contributors

Milan Skocic

3.1.4 Commits

Full Changelog: https://github.com/MilanSkocic/pyecx/compare/....0.1.0

CHAPTER

FOUR

AUTOGENERATED DOCUMENTATION

4.1 ecx

4.1.1 Fortran

Fortran code API

4.1.2 C API

Common headers

- *ecx_types.h*

```
/**
 * @file ecx_types.h
 * @brief Type C header for th ecx library.
 * @details Compatibilty layer for handling complex numbers with MSC.
 * It is imported by all headers for each submodule.
 */
#ifndef ECX_TYPES_H
#define ECX_TYPES_H

#include <complex.h>
#if _MSC_VER
typedef _Dcomplex ecx_cdouble; /**< Cross platform complex type. */
#define ecx_cbuild(real, imag) (_Cbuild(real, imag))/**< Cross platform complex type␣
↪constructor*/
#else
typedef double _Complex ecx_cdouble; /**< Cross platform complex type. */
#define ecx_cbuild(real, imag) (real+I*imag) /**< Cross platform complex type␣
↪constructor*/
#endif

#endif
```

- *ecx.h*

```
/**
 * @file ecx.h
 * @brief Main C header for th ecx library.
 * @details Includes all the headers for each submodule.
 */
#ifndef ECX_H
#define ECX_H
```

(continues on next page)

(continued from previous page)

```
#include "ecx_core.h"
#include "ecx_eis.h"
#include "ecx_pec.h"
#include "ecx_kinetics.h"

#endif
```

EIS headers

```
/**
 * @file ecx_eis_capi.h
 * @brief EIS C header for th ecx library.
 * @details Complex impedance
 */
#ifndef ECX_EIS_CAPI_H
#define ECX_EIS_CAPI_H
#include "ecx_types.h"
#include "ecx_core.h"

extern void ecx_capi_zr(double *w, double R, size_t n, ecx_cdouble *Z);
extern void ecx_capi_zc(double *w, double C, size_t n, ecx_cdouble *Z);
extern void ecx_capi_zl(double *w, double L, size_t n, ecx_cdouble *Z);
extern void ecx_capi_zcpe(double *w, double Q, double a, size_t n, ecx_cdouble *Z);
extern void ecx_capi_zw(double *w, double s, size_t n, ecx_cdouble *Z);
extern void ecx_eis_capi_z(double *p, double *w, ecx_cdouble *z, char e, size_t k,␣
↪size_t n, int *errstat);

#endif
```

PEC headers

```
/**
 * @file ecx_pec_capi.h
 * @brief EIS C header for th ecx library.
 */
#ifndef ECX_PEC_CAPI_H
#define ECX_PEC_CAPI_H
#include "ecx_types.h"
#include "ecx_core.h"


#endif
```

4.2 pyipaws

C extension wrapping the EIS module of the Fortran ecx library.

pyecx.eis.z()

z(e, w, p)–>memview

Compute the complex impedance of the element e.

BIBLIOGRAPHY

[1] Evgenij Barsoukov and J.R. Macdonald. *Impedance Spectroscopy: Theory, Experiment, and Applications*. John Wiley & Sons, Inc., Hoboken, NJ, USA, second edition, 2005.

[2] Mark E. Orazem and Bernard Tribollet. *Electrochemical Impedance Spectroscopy*. John Wiley & Sons, Inc., 2008. ISBN 978-0-470-04140-6.

[3] B.A. Boukamp. A Nonlinear Least Squares Fit Procedure for Analysis of Immittance Data of Electrochemical Systems. *Solid State Ionics*, pages 31–44, 1986.

[4] Philip R. Bevington and D. Keith Robinson. *Data Reduction and Error Analysis for Physical Sciences*. McGraw Hill, New York, third edition, 2003. ISBN 0-07-247227-8.

[5] William H. Press, Saul A. Teukolsky, William T. Vetterling, and Brian P. Flannery. *Numerical Recipes: The Art of Scientific Computing*. Cambridge University Press, Cambridge, third edition, 2007.

[6] E. Becquerel. Mémoire sur les effets électriques produits sous l'influence des rayons solaires. *Comptes Rendus des Séances Hebdomadaires*, 9:561–567, 1839.

[7] Ulrich Stimming. Photoelectrochemical studies of passive films. *Electrochimica Acta*, 31(4):415–429, 1986.

[8] H Gerischer. Electrochemical Behavior of Semiconductors under Illumination. *Journal of The Electrochemical Society*, 113(11):1174–1182, 1966.

[9] \relax A. Wallace Copeland, Otis D. Black, and A. B. Garrett. The Photovoltaic Effect. *Chemical Reviews*, 31(1):177–226, 1942. doi:10.1021/cr60098a004.

[10] S R Morrison. *Electrochemistry at Semiconductor and Oxidized Metal Electrodes*. Plenum Press, New York, 1980.

[11] H Gerischer. Semiconductor electrodes and their interaction with light. In Mario Schiavello, editor, *Photoelectrochemistry, Photocatalysis and Photoreactor*, pages 39–106. D. Reidel Publishing Company, Dordrecht, 1985.

[12] R Memming. *Semiconductor Electrochemistry*. WILEY-VCH Verlag GmbH, Weinheim, 2008.

[13] P. Marcus and F Mansfield. *Analytical Methods in Corrosion Science and Engineering*. CRC Press, Boca Raton, FL, 2006.

[14] Allen J. Bard and M. Stratmann. *Fundamentals of Semiconductors Electrochemistry and Photoelectrochemistry*. Wiley-VCH, 2002.

[15] Norio Sato. *Electrochemistry at Metal and Semiconductors Electrodes*. Elsevier Science, Amsterdam, 1998.

[16] Jean-Francis Marucco. *Chimie Des Solides*. EDP Sciences, Paris, 2006. ISBN 978-2-86883-673-1.

[17] Wolfgang W Gärtner. Depletion-Layer Photoeffects in Semiconductors. *Physical Review*, 116(1):84–87, 1959.

[18] M. Butler. Photoelectrolysis and physical properties of the semiconducting electrode WO\textsubscript 3. *Journal of Applied Physics*, 48(5):1914, 1977. doi:10.1063/1.323948.

PYTHON MODULE INDEX

p

INDEX